Cell Reports

Article

Long interspersed nuclear elements safeguard neural progenitors from precocious differentiation

Graphical abstract

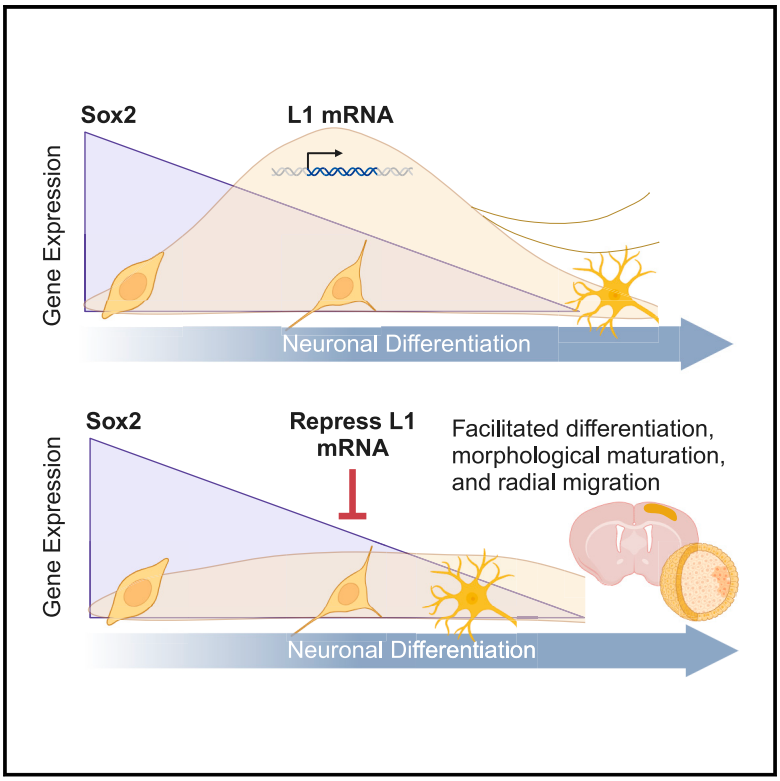

Authors

Tomohisa Toda, Tracy A. Bedrosian, Simon T. Schafer, ..., Matthieu Boulard, Sarah L. Parylak, Fred H. Gage

Correspondence

tomohisa.toda@fau.de (T.T.), gage@salk.edu (F.H.G.)

In brief

Toda et al. find that long interspersed nuclear element-1 (L1 or LINE-1) regulates the maintenance of neural progenitor pools during brain development. The study highlights unrecognized physiological roles for repetitive elements in the genome during brain development and their potential impact on brain evolution.

Highlights

- L1s are dynamically expressed during neural differentiation
- L1s are required to maintain neural progenitor pools in mice and humans
- L1s regulate neural differentiation in a retrotransposition-independent manner

Toda et al., 2024, Cell Reports *43*, 113774
February 27, 2024
https://doi.org/10.1016/j.celrep.2024.113774

CellPress

Cell Reports

CellPress
OPEN ACCESS

Article

Long interspersed nuclear elements safeguard neural progenitors from precocious differentiation

Tomohisa Toda,[1,2,3,10,*] Tracy A. Bedrosian,[1,4,10] Simon T. Schafer,[1,5,6,10] Michael S. Cuoco,[1,8,9] Sara B. Linker,[1] Saeed Ghassemzadeh,[1] Lisa Mitchell,[1] Jack T. Whiteley,[1] Nicole Novaresi,[1] Aidan H. McDonald,[1] Iryna S. Gallina,[1] Hyojung Yoon,[4] Mark E. Hester,[4] Monique Pena,[1,5,6] Christina Lim,[1] Emelia Suljic,[1] Abed AlFatah Mansour,[1] Matthieu Boulard,[7] Sarah L. Parylak,[1] and Fred H. Gage[1,11,*]

[1]Laboratory of Genetics, The Salk Institute for Biological Studies, 10010 North Torrey Pines Road, La Jolla, CA 92037, USA
[2]Laboratory of Neural Epigenomics, Institute of Medical Physics and Micro-tissue Engineering, Friedrich-Alexander-Universität Erlangen-Nürnberg, 91054 Erlangen, Germany
[3]Nuclear Architecture in Neural Plasticity and Aging Laboratory, German Center for Neurodegenerative Diseases, 01307 Dresden, Germany
[4]Institute for Genomic Medicine, Nationwide Children's Hospital, Columbus, OH 43205, USA
[5]Department of Psychiatry and Psychotherapy, School of Medicine and Health, Technical University of Munich, Munich, Germany
[6]TUM Center for Organoid Systems (COS), Munich Institute of Biomedical Engineering, Garching, Germany
[7]Epigenetics & Neurobiology Unit, EMBL Rome, European Molecular Biology Laboratory, Via Ramarini 32, 00015 Monterotondo, Italy
[8]Computational Neural DNA Dynamics Lab, Department of Cognitive Science, University of California, San Diego, San Diego, CA, USA
[9]Bioinformatics and Systems Biology Graduate Program, University of California, San Diego, San Diego, CA, USA
[10]These authors contributed equally
[11]Lead contact
*Correspondence: tomohisa.toda@fau.de (T.T.), gage@salk.edu (F.H.G.)
https://doi.org/10.1016/j.celrep.2024.113774

SUMMARY

Long interspersed nuclear element-1 (L1 or LINE-1) is a highly abundant mobile genetic element in both humans and mice, comprising almost 20% of each genome. L1s are silenced by several mechanisms, as their uncontrolled expression has the potential to induce genomic instability. However, L1s are paradoxically expressed at high levels in differentiating neural progenitor cells. Using *in vitro* and *in vivo* techniques to modulate L1 expression, we report that L1s play a critical role in both human and mouse brain development by regulating the rate of neural differentiation in a reverse-transcription-independent manner.

INTRODUCTION

Repetitive elements compose more than half of the human genome. One of the most abundant of these elements is long interspersed nuclear element-1 (L1 or LINE-1), a retrotransposon that self-replicates and accounts for almost 20% of human and mouse genomes. Only a fraction of L1 elements are capable of active retrotransposition, but in doing so, they can create *de novo* mutations, induce genomic instability, and disrupt the transcription of neighbor genes.[1–5] Because of its risk for deleterious effects on the genome, L1's promoters are epigenetically repressed in most cell types by DNA methylation and associated heterochromatin. Recent findings further highlighted deleterious roles of L1 cDNA and RNA in cellular senescence,[6–8] suggesting that L1s have various impacts at different levels. Paradoxically, however, L1 expression rises dramatically in neural progenitor cells (NPCs) during differentiation, raising the possibility that L1 may have unexplored physiological roles in neurodevelopment.[9]

Here, we investigated the possibility that L1 expression plays a role in the regulation of NPCs. During brain development, NPCs give rise to both neurons and glial cells in a tightly regulated process that must balance proliferation and differentiation. A complex interplay of genetic and molecular factors, which are still incompletely understood, ensures that cells are generated, migrate, and mature at the correct times and locations. In the present study, we provide evidence that knockdown of *L1* transcripts induces precocious neural differentiation and that simultaneous exogenous expression of L1s can prevent precocious differentiation in mouse NPCs. Further, an L1 mutant without reverse transcription activity can rescue L1-knockdown-induced neural differentiation, suggesting that the underlying mechanism is reverse-transcription independent. In differentiating conditions, the knockdown of *L1* transcripts did not affect neuronal differentiation but reduced glial differentiation, suggesting potential roles in the regulation of glial fate commitment in addition to the maintenance of NPCs. We also show that knockdown of *L1* transcripts in human cerebral organoids induces differentiation, suggesting evolutionarily conserved roles for L1s in neural development. Altogether, our findings suggest that L1s play physiological roles in the regulation of brain development.

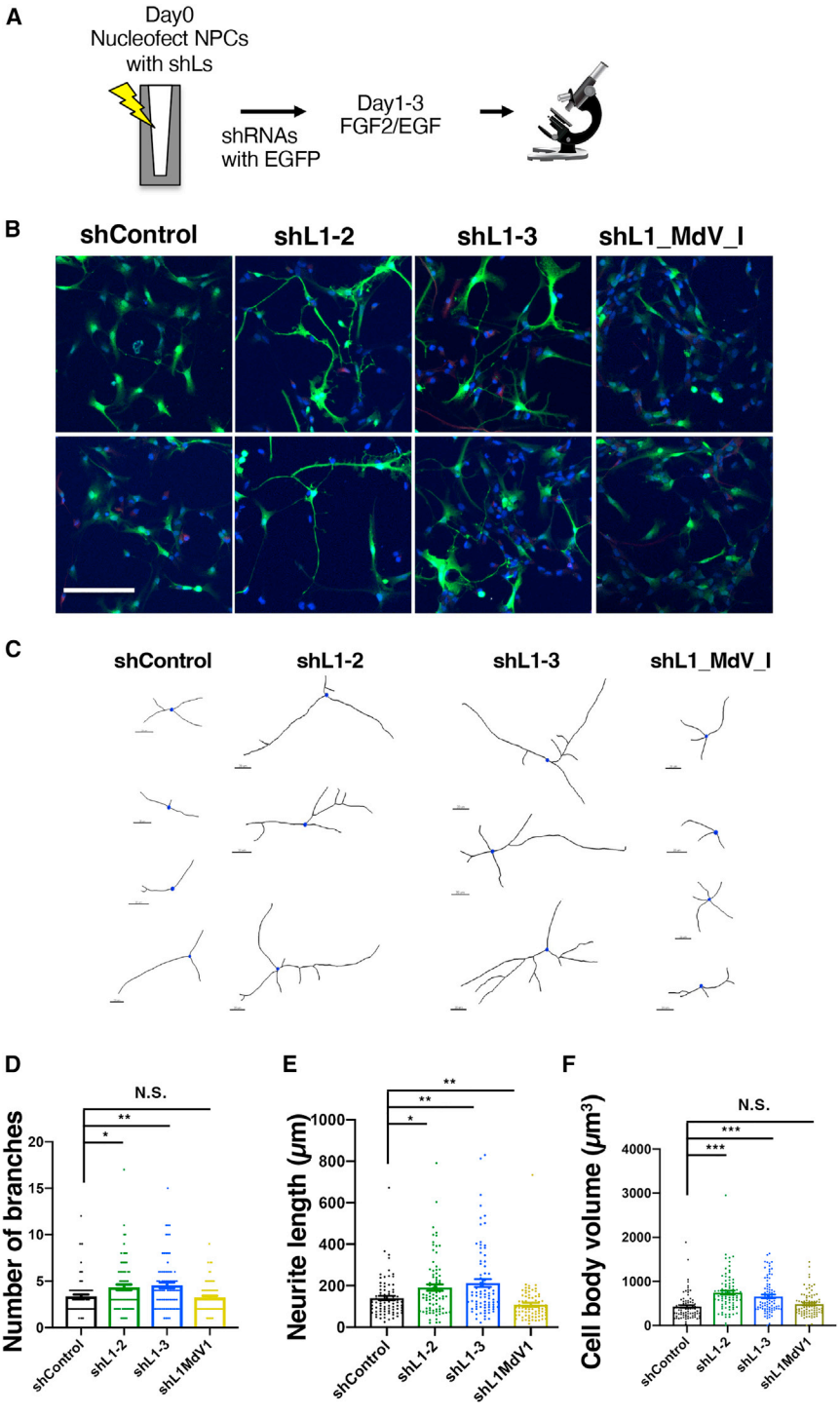

Figure 1. Downregulation of L1 in NPCs facilitates morphological differentiation

(A) A schema of the experimental design.

(B) Morphological differentiation of mouse NPCs in a proliferative culture condition 3 days after introduction of shRNAs with GFP. Scale bar, 100 μm.

(C) Reconstructions of cell morphology with Imaris after shRNA treatment. Cell bodies are shown in blue, and neurites are shown in black. Scale bars, 20 μm.

(D) Number of neurite branches on GFP-positive cells. Mann-Whitney test, $^{**}p < 0.01$ and $^{*}p < 0.05$.

(E) Total neurite length on GFP-positive cells. Mann-Whitney test, $^{**}p < 0.01$ and $^{*}p < 0.05$.

(F) Cell body volume of GFP-positive cells. Mann-Whitney test, $^{***}p < 0.001$.

Data are presented as mean ± SEM. n = 80 cells from four experiments. The shControl condition was used for statistical comparison.

RESULTS

Downregulation of L1s facilitates neural differentiation

First, to examine the role of L1 expression in mouse NPCs, we designed short hairpin RNAs (shRNAs) targeting active L1 families in the mouse genome (L1MdA_I, L1MdTf_I, and L1MdGf_I; Figure S1A).[10] Full-length L1 elements are composed of two open reading frames (ORFs), ORF1 and ORF2. Specific small interfering RNA (siRNA) sequences targeting either ORF from the common sequences of active L1s were selected using siDirect 2.0.[11] Four siRNA sequences shared by L1MdA_I, L1MdTf_I, and L1MdGf_I were chosen, and shRNAs (shL1s) were constructed based on the siRNA sequence (Figure S1A). The chosen shRNAs were largely predicted to target transcripts of the intended L1 subfamilies with limited off targets (Figure S1B). To understand the expression pattern of L1 elements during neural development, we quantified L1 expression from published RNA sequencing (RNA-seq) data from NPCs and neurons using L1EM.[12,13] We found that L1MdA_1 and L1MdTf_1 transcripts were highly expressed in NPCs as expected, but other L1 subfamilies were expressed at relatively low levels in NPCs (Figure S1C). Intriguingly, L1MdA_1 levels were downregulated in neurons, whereas L1MdTf_1 levels were further upregulated in neurons, indicating that the expression dynamics of L1 elements are distinct among different L1 subfamilies and that each L1 subfamily might receive distinct regulation of its expression. Downregulation of L1 expression after the introduction of shL1s in mouse NPCs was verified by real-time qPCR with primers previously designed to detect active L1s[14] (Figures S2A and S2B). Downregulation of L1MdTf_1 by shL1-2 was also confirmed by RNA-seq using L1EM (Figures S2C and S2D). Furthermore, the shRNAs also downregulated the levels of Orf1 protein in mouse NPCs (Figures S2E and S2F), indicating that shL1s resulted in an inhibition of L1's RNA translation.

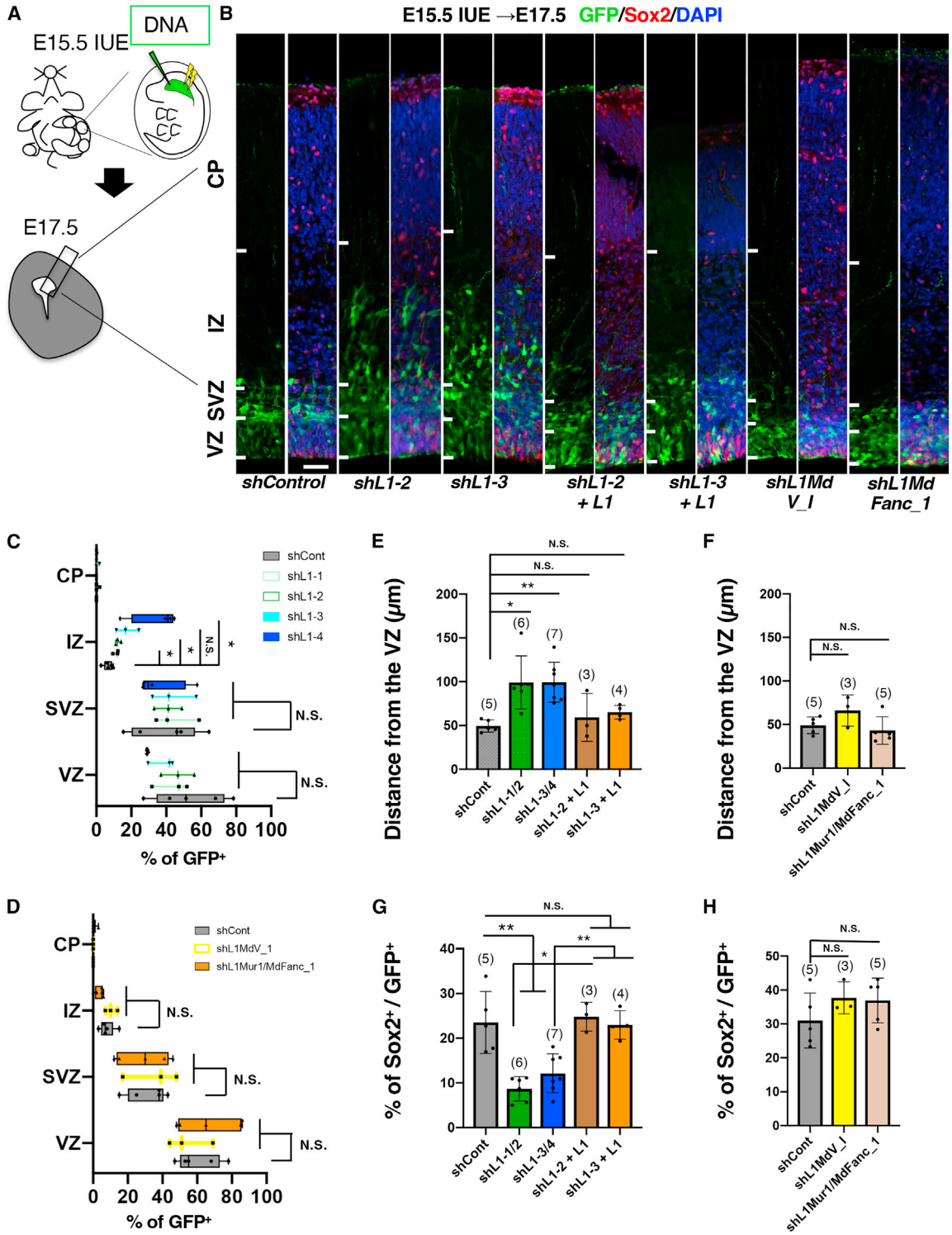

Figure 2. L1 regulates radial migration in the developing cortex

(A) A schema of the IUE procedure used to manipulate the levels of L1 in the developing cerebral cortex. GFP with shRNAs was introduced into the cerebral cortex at E15.5, and brains were collected at E17.5.

(B) Coronal sections of the brains were stained with anti-Sox2 antibody, anti-GFP antibody, and DAPI. VZ, ventricular zone; SVZ, subventricular zone; IZ, intermediate zone; CP, cortical plate. Scale bar: 35 μm.

(legend continued on next page)

After the introduction of shL1s, mouse NPCs were maintained in proliferative culture conditions with FGF2 and EGF to address the role of L1s in the maintenance of the NPC state. The introduction of shL1s induced drastic morphological differentiation in mouse NPCs (Figures 1A and 1B). Consistent phenotypes were observed with two other shL1s (shL1-1 and shL1-4). Quantitative analyses revealed that knockdown of L1 expression facilitated neurite branching and neurite extensions (Figures 1C–1F). Furthermore, knockdown of L1s induced filopodia-like structures on neurites 3 days after the introduction of shL1s (Figure S2G). These data suggest that L1 expression is critical for the maintenance of mouse NPCs and that downregulation of L1 expression induces morphological differentiation even under proliferative culture conditions for NPCs. These effects are specific to shRNAs targeting active L1s because shRNA targeting inactive L1s (L1MdV_I) did not affect cellular morphology (Figure 1). Consistent with these results, knockdown of L1s downregulated the expression of Ki67 (Figures S3A and S3B), a mitotic cell marker, suggesting that down-regulation of L1 expression reduced proliferating NPCs before the reduction of NPC marker expression (Figures S3C–S3E). Importantly, the L1-knockdown-induced phenotype was efficiently rescued by coexpression of an shRNA-resistant full-length L1[15] (Figure S4). These results indicate that the observed induction of neural differentiation is caused by the deficiency in L1 expression, and L1 expression is essential to maintain the state of NPCs.

L1s regulate neural differentiation in the developing neocortex

Next, to test whether L1s play critical roles in the developing brain *in vivo*, we introduced shL1s using *in utero* electroporation (IUE).[16–18] shL1s were introduced at embryonic day 15.5 (E15.5), and the cerebral cortices were analyzed 2 days later at E17.5 (Figure 2A). In controls, most of the GFP-positive cells were located within the ventricular zone (VZ) and the subventricular zone (SVZ) of the developing cerebral cortex (Figure 2B). Consistent with the results obtained *in vitro*, treatment with shRNAs targeting active L1s promoted precocious radial migration, with significantly higher numbers of GFP-positive cells present in the intermediate zone as compared to controls (Figures 2B, 2C, and 2E). These findings suggest that knockdown of L1s from NPCs *in vivo* causes accelerated radial migration, which is a critical process during brain development.[19] In line with these findings, knockdown of active L1s reduced the proportion of Sox2-positive cells colocalized with GFP-positive cells in the developing cortex (Figure 2G). These results are consistent with the idea that the knockdown of L1s facilitates a neural differentiation program. On the other hand, the introduction of shRNAs targeting inactive L1s (shL1MdV_1, shL1Mur1, and shL1MdFanc_1) affected neither radial migration (Figures 2B, 2D, and 2F) nor the proportion of Sox2-positive cells among GFP-positive cells (Figure 2H). Importantly, the effects of L1 knockdown were reversed by the simultaneous introduction of full-length L1 (Figures 2B, 2E, and 2G), indicating that the expression of active L1s plays a critical role in the maintenance of mouse NPCs *in vivo* and that knockdown of L1s induces precocious differentiation.

Reverse-transcription-independent roles of L1 in neural development

To gain further insight into L1 function in the developing cortex, we used IUE to exogenously overexpress wild-type L1 (WT-L1) in the developing cortex *in vivo*. Exogenous expression of WT-L1 markedly retained GFP-positive cells in the VZ compared to controls (Figures 3A and 3B), suggesting that L1 expression maintains NPCs and inhibits radial migration. Consistent with these results, the proportion of Sox2-positive cells colocalized with GFP-positive cells was higher when full-length L1 was introduced (Figure 3F). L1 Orf2 encodes a reverse transcriptase (RT) that has been implicated in the regulation of differentiation as well as genomic mosaicism.[20] To determine whether the functional involvement of L1s in NPCs was dependent on its RT activity, we cotransfected mutated L1 lacking RT activity (mL1) with shL1s. mL1 reversed the effect of shL1s similar to full-length L1 (Figures 3C, 3E, and 3G). These findings suggest that L1 expression regulates NPCs in an RT-activity-independent manner.

To gain further mechanistic insight into the role of L1's expression in neural progenitors, we analyzed genome-wide transcriptional consequences of L1 knockdown using RNA-seq. To identify genes regulated by active L1s, we focused on those differentially regulated in response to shL1s targeting active L1 elements, and reversed by WT-L1, but not affected by shL1 targeting inactive L1s. A total of 477 genes were associated with the manipulation of active L1s ($p < 0.05$) (Figure S5A). To verify the specificity of L1 manipulation, we investigated whether L1-regulated genes contained putative shL1 target sequences. Of 477 differentially expressed genes (L1-DEGs), only 18 contained putative shL1 target sequences (Figure S5B), suggesting that most of the L1-DEGs were not directly targeted by shL1s (shL1-2 $p = 0.87$, shL1-3 $p = 0.47$).

Subsequently, we examined whether genes containing putative shL1 sequences within introns or exons were affected by the manipulation of L1s, but the presence of putative shL1

(C) Distribution of GFP-positive cells in L1-knockdown brains at E17.5. Welch's *t* test with Benjamini and Hochberg correction. *$p < 0.05$, n = 3–5 animals. The shControl condition was used for statistical comparison.
(D) Distribution of GFP-positive cells in brains treated with shRNA targeting inactive L1. Welch's *t* test. n = 3–5.
(E) Mean migration distance of GFP-positive cells from the VZ in L1-knockdown brains. One-way ANOVA ($p = 0.0023$), followed by Tukey-Kramer, **$p < 0.01$ and *$p < 0.05$.
(F) Mean migration distance from the VZ in brains treated with shRNA targeting inactive L1. Student's t test with Benjamini and Hochberg correction.
(G) Proportion of Sox2-positive cells in GFP-positive cells in L1-knockdown brains. One-way ANOVA ($p = 0.0001$), followed by Tukey-Kramer, *$p < 0.05$ and **$p < 0.01$.
(H) Proportion of Sox2-positive cells in GFP-positive cells in brains treated with shRNA targeting inactive L1. Student's t test with Benjamini and Hochberg correction.
The numbers of animals are indicated in parentheses unless otherwise indicated in the legend. Data are presented as mean ± SD. N.S., not significant.

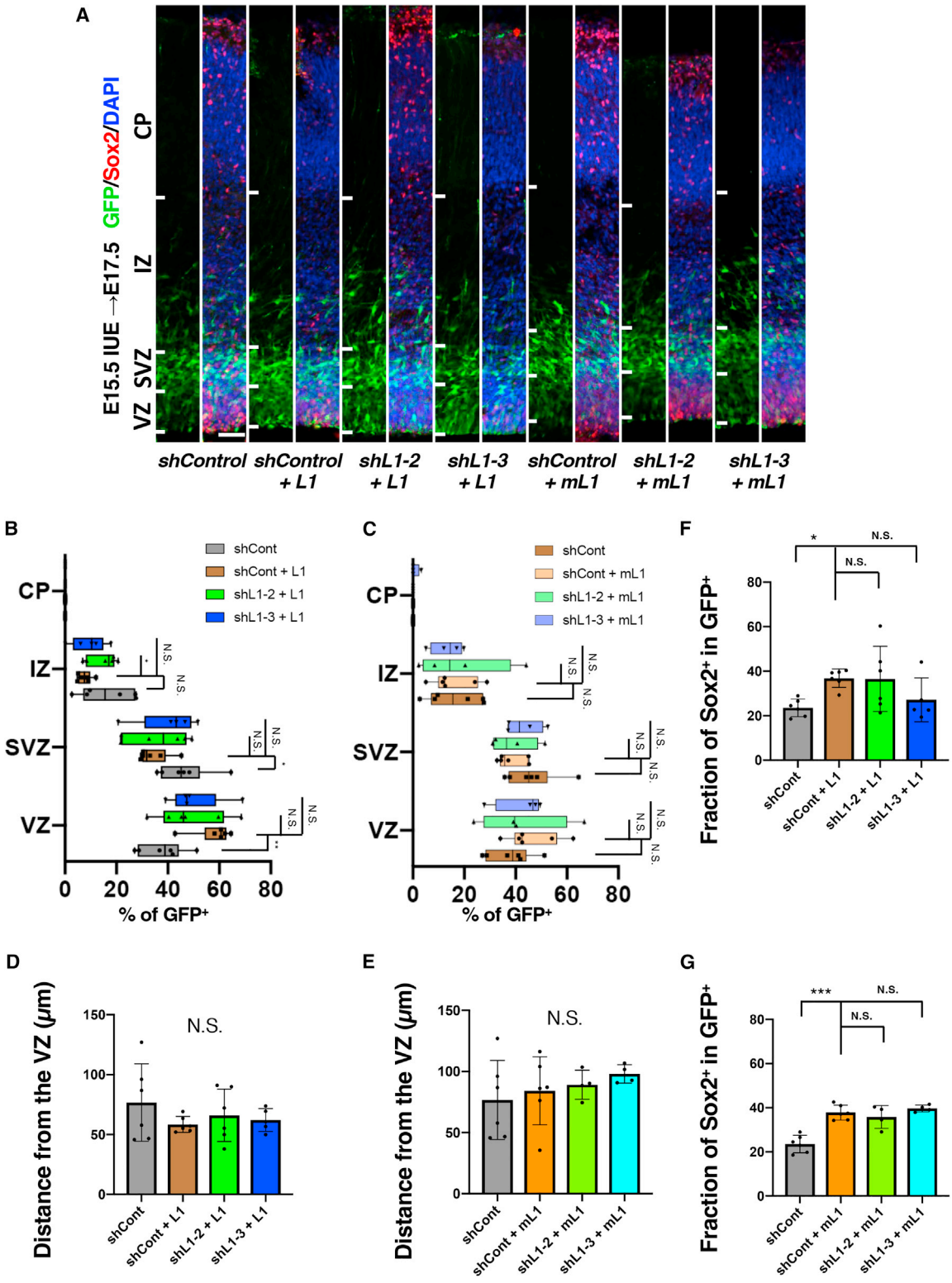

Figure 3. Exogenous expression of L1 maintains NPCs

(A) Coronal sections of the brains were prepared and stained with anti-Sox2 antibody, anti-GFP antibody, and DAPI. Note that full-length L1 (L1) expression rescued shL1-induced radial migration. Scale bar: 35 μm. VZ, ventricular zone; SVZ, subventricular zone; IZ, intermediate zone; CP, cortical plate.

(legend continued on next page)

sequences within genes showed negligible effects on their expression (Figure S5C). We also examined *cis* effects of shL1s on genes close to putative shL1 sequences. The spatial relationship between the distance from plausible shL1 targeting sequences to promoters of genes and the change in the corresponding gene's expression showed small but significant effects (shL1-2, $R^2 = -0.11$, $p < 1.88e{-}05$; shL1-3, $R^2 = -0.07$, $p < 2.6e{-}03$), indicating that while there is no direct effect on gene expression, there may be a small *trans* effect of L1 expression in the local genomic region (Figure S5D). Together, these results support the conclusion that the transcriptomic changes are mediated by L1s but not by the mistargeted effects of shL1s. L1-DEGs showed signatures of enrichment in the regulation of cell morphogenesis or projection, consistent with our observations (Figure S5E). Interestingly, expression of a collagen gene (*Col18a1*) was associated with the expression level of active L1s (Figure S5F).

The change in the expression of collagen levels was previously implicated in the evolution of neocortex.[21] We tested whether *L1* mRNA was capable of interacting with chromatin to directly regulate L1-DEGs, as shown in a recent report.[22] Using chromatin isolation by RNA purification for L1spa, we found that *L1* mRNA interacted with L1 chromatin as previously shown.[22] However, we did not observe any evidence of such interactions with regard to selected genes that were differentially expressed due to modulation of L1 expression (L1-DEGs) such as *Tle3* or *Fgfr2* (Figure S5G). Taken together, our observations suggest that active L1s regulate the differentiation of NPCs through the modulation of gene expression and that the effect on differentiation occurs in an RT-independent manner.

L1s are dispensable for neuronal commitment but potentially critical for gliogenesis

We then addressed the role of L1s in fate commitment upon differentiation. L1 shRNAs were introduced to mouse NPCs by nucleofection, and EGF was withdrawn upon plating to facilitate differentiation *in vitro* (Figure 4A). Three days after the plating, the expression of neuronal markers (Tuj1, Map2), a glial marker (GFAP), and a mitotic marker (Ki67) was analyzed (Figures 4B–4F). The fractions of Tuj1, Map2, and Ki67 did not show significant changes ($p > 0.05$, ANOVA), indicating that the expression of L1s is dispensable for neuronal commitment or maintenance of proliferation in the differentiating condition. Intriguingly, the proportion of GFAP-positive cells was significantly decreased (*$p < 0.05$, ANOVA), indicating a potential role for L1s in the regulation of astrocyte differentiation or maturation.

Next, to investigate the role of L1s in neuronal maturation *in vivo*, shL1s were administered by IUE at E15.5, and brains were collected at postnatal day 7. To compare neuronal morphological maturation, morphology of GFP-positive cortical neurons in layer 2/3 of the primary somatosensory cortex was examined (Figures 4G and 4H).[23] Cell area and dendritic length were not significantly different between shControl and shL1s (Figures 4I and 4J) ($p > 0.05$, Kruskal-Wallis). On the other hand, the number of dendritic branches was markedly increased in shL1-introduced GFP-positive cells (*$p < 0.05$, Kruskal-Wallis) (Figure 4K). These data indicate two possibilities: knockdown of L1s induced earlier differentiation from NPCs, or the entire developmental process was shifted in advance. Alternatively, L1s may be involved in the regulation of neuronal morphological maturation.

L1s regulate neural differentiation in human cortical organoids

Finally, to test whether the role of L1s in the maintenance of NPCs is evolutionarily conserved, we generated human forebrain organoids derived from subject-derived pluripotent stem cells to model human-specific aspects of early corticogenesis.[24,25] We designed a set of shRNAs specifically targeting active human L1s. Unique sequences of active human L1 (L1HS) and inactive human L1 (L1M) were computationally selected, and siRNA sequences targeting ORF1 and ORF2 of L1HS and L1M were designed using siDirect 2.0 (shL1HS-1, shL1HS-2, and shL1M). The L1 subfamilies in the human genome potentially targeted by shRNAs were estimated (Figure S6A). Based on the siRNA sequences, shRNAs were constructed and their effects were verified using real-time qPCR and western blotting (Figure S6). Forebrain organoids were generated using both H1 embryonic stem cells and induced pluripotent stem cells (iPSCs) derived from healthy subjects. To efficiently introduce shRNAs into NPCs within developing forebrain organoids, we labeled dividing radial glia-like cells (RGLs) using a GFP-expressing retrovirus with shRNAs (Figure 5A). This approach allowed us to follow the progenies of labeled RGLs as they migrated and integrated into the evolving cortical plate (CP) (Figure 5B). Strikingly, the distribution of retrovirally labeled RGLs 3 days post-infection (3 dpi) showed marked differences between L1-deficient (shL1HS-1 and shL1HS-2) cells and controls, with GFP-positive L1-deficient cells observed more frequently in the CP-like regions (Figures 5B and 5C). In line with this finding, quantitative assessment of their migratory positions at 3 dpi showed a significantly shifted migratory advancement of immature neurons deficient for L1s (shL1HS-1 and shL1HS-2) toward the pial surface within CP-like regions of the developing human organoid as compared to controls (Figures 5D and 5E).

To validate these observations in an independent setting, we optimized an electroporation paradigm to target plasmids expressing the same target shRNAs to RGL-like cells in a

(B) Rescue of the distribution of GFP-positive cells in the L1-knockdown brains by full-length L1 (L1) at E17.5. Student's t test with Benjamini and Hochberg correction. *$p < 0.05$ and **$p < 0.01$. n = 5–6. The shControl + L1 condition was used for statistical comparison.
(C) Rescue of the distribution of GFP-positive cells in the L1-knockdown brains by mutated L1 (mut-L1) lacking reverse transcriptase activity at E17.5. Student's t test. n = 4–6.
(D) Mean migration distance of GFP-positive cells from the VZ in brains treated with shL1 + L1. One-way ANOVA ($p = 0.46$). n = 5–6.
(E) Mean migration distance of GFP-positive cells from the VZ in brains treated with shL1 + mut-L1. One-way ANOVA ($p = 0.60$). n = 4–6.
(F) Proportion of Sox2-positive cells in GFP-positive cells. Steel-Dwass test ($p < 0.05$), *$p < 0.05$.
(G) Proportion of Sox2-positive cells in GFP-positive cells. One-way ANOVA ($p = 8.5377e{-}06$).
Data are presented as mean ± SD (***$p < 0.001$). N.S., not significant.

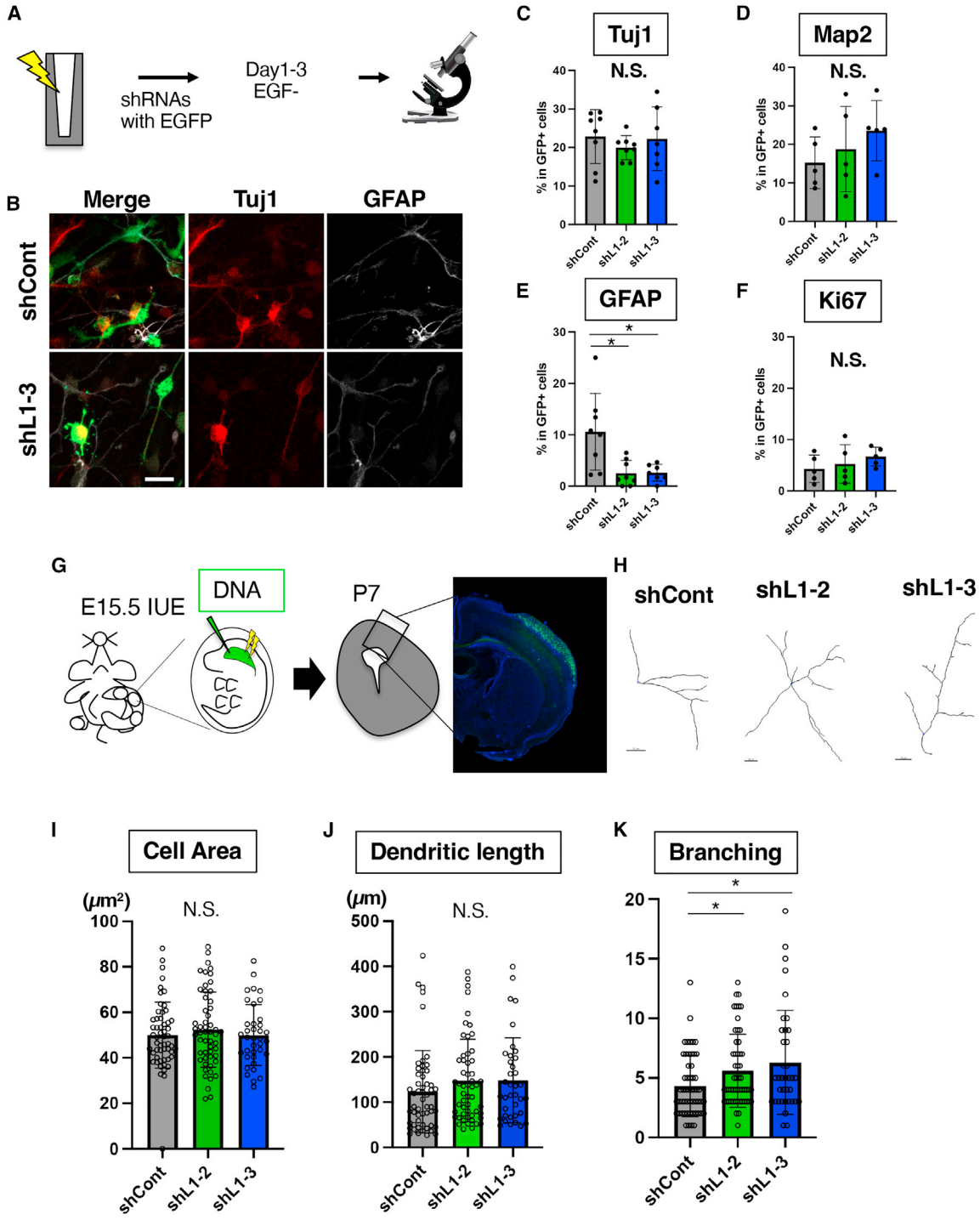

Figure 4. Effects of L1 inhibition on neural differentiation and morphological maturation

(A) Experiment schema for neural differentiation after the introduction of shL1s.

(B) Representative images 3 days after shL1 introduction in differentiation cells from NPCs. Scale bar, 20 μm.

(C–F) Quantification of GFP-positive cells with markers. ANOVA followed by Holm-Sidak's multiple comparisons test, *p < 0.05. n = 5–8 experiments.

(G) Schematic diagram of IUE experiments for mice.

(legend continued on next page)

virus-independent manner. Plasmids were injected into the ventricles and then introduced via electroporation (Figure S7A). We chose 5- to 6-week-old forebrain organoids for electroporation because a strong expression of GFP was consistently observed in the VZ-like regions at this time point. In control samples at 3 days post-electroporation, the majority of GFP-positive cells were located within the VZ-like regions (Figure S7B). When shL1HS-1 and shL1HS-2 were introduced, GFP-positive cells migrated further out from the VZ, and some of them migrated into the CP-like structure (Figures S7B–S7D). This enhanced migration was not evident when shL1M was introduced, suggesting that the effect of L1 knockdown was specific for active L1s. Thus, knockdown of L1s in the VZ of human cerebral organoids also facilitates the differentiation of NPCs.

Subsequently, we tested whether L1s are involved in fate commitment and neuronal maturation. To address this point, we first applied retroviruses harboring shL1s in 4-week-old human cortical organoids and collected them 2 weeks after retroviral application (Figures S7E and S7F). At this developmental time point, 80% of shControl-expressing GFP-positive cells became CTIP2 positive, a marker for deep-layer cortical neurons (Figures S7E and S7F). In shL1s-expressing samples, no significant changes in the fraction of CTIP2-positive cells were observed (Figure S7F), indicating that L1s are dispensable for neuronal commitment from NPCs to deep-cortical-layer neurons in the human cortical organoid system. To further assess morphological maturation of neurons, shL1s were introduced by electroporation, which allowed us to sparsely label cells, and the electroporated cells were examined 2 weeks after the electroporation (Figure 5F). Intriguingly, shLHS-1-treated cells showed significantly longer total dendrite length (Figures 5F and 5G; ***$p = 0.0017$, Mann-Whitney test) and higher dendritic complexities as compared to the control group (Figure 5H). These data indicate that L1 elements consistently play critical roles in neuronal morphological maturation both in rodents and human.

DISCUSSION

Expression of L1s is largely believed to be detrimental due to the risk of insertional mutagenesis, transcriptional interference, and genomic instability. In fact, recent evidence uncovered pathological roles of L1 in the aging cells or age-related neurological diseases.[6,8,26] The findings indicated that de-repression of L1s causes cellular senescence, heterochromatin disorganization, and cell death. Nevertheless, our results demonstrate that L1 expression in NPCs plays a critical role in regulating normal neural differentiation. Our finding supports the idea that L1 expression itself plays a role in early developmental processes.[22] Furthermore, our data show that the role of L1 expression in neural development is evolutionarily conserved in rodents and humans. To address the role of L1s, we employed a knockdown strategy. We initially attempted knocking out the putatively active L1s copies by a CRISPR-Cas9 approach during mouse early embryonic development, but embryos did not develop, perhaps due to excessive DNA damage. Therefore, we were not able to investigate the effects of L1 knockout on cortical development. To probe the function of L1 transcription, we employed a knockdown strategy using shRNA. We ruled out off-target effects since independent sets of shRNA designs (i.e., mouse and human) induced similar effects in both model systems and could be rescued by exogenous expression of L1. Despite abundant L1 transcripts in differentiating NPCs, most of these RNAs were not retrotransposed, even if somatic L1 insertions could occur in the neuronal lineage.[27–30] Therefore, the physiological roles of L1s in brain development have been largely unknown. Based on our findings, we propose that one of the physiological roles of L1s in the developing brain is to safeguard NPCs from precocious differentiation. Increasing evidence supports the hypothesis that human-specific features are derived from a delayed developmental process, a process called neoteny.[31–33] Since the expression of L1s in NPCs contributes to the temporal regulation of brain development, L1 expression may be involved in the emergence of neotenic features in brain evolution.

The exact molecular mechanisms underlying the regulation of NPCs by L1s remain elusive, but our data indicate that retrotransposition is dispensable. Interestingly, L1 exerts its effect at various levels of cDNA, RNA, and local transcription, and L1 expression has been shown to regulate global chromatin accessibility in early mouse embryos.[34] Furthermore, L1 mRNA is involved in the regulation of ribosomal RNA expression and the cellular state of early mouse embryos by acting as long non-coding RNA.[22] Similar to its roles in early embryonic development, our data suggest L1s modulate gene networks in NPCs to regulate brain development. In agreement with our study, two recent independent studies also uncovered essential roles of L1s in brain development. Mangoni and colleagues recently showed that L1 expression is essential for the maintenance of NPCs during development of the mouse cortex and that L1 mRNAs likely regulate the genetic programs of NPCs through interactions with the Polycomb repressive complex 2.[35] Garza and colleagues showed that L1s are dynamically expressed during human brain development. Using the published RNA-seq dataset,[36] we have independently analyzed L1 expression patterns from human iPSCs through NPCs to neurons *in vitro*. We consistently observed dynamic expression patterns of L1 subfamilies during neural differentiation (Figure S8). Garza and colleagues further uncovered that human-specific L1s could regulate brain development through *trans* effects on the expression of neighboring long non-coding RNAs.[37] These studies consistently indicate essential roles for L1 expression in the maintenance of NPCs both in rodent and human models, albeit through different potential mechanisms. These observations suggest that, during

(H) Representative images of dendritic morphology of electroporated neurons in layer 2/3 of the primary somatosensory cortex in postnatal day 7 (P7) mice. Scale bars: 10 μm.

(I–K) Quantification of cell area, dendritic length, and branching numbers of dendrite from electroporated cells at P7. ANOVA followed by Holm-Sidak's multiple comparisons test, *$p < 0.05$. 37–54 cells from 3 experiments.

Data are presented as mean ± SD. N.S., not significant.

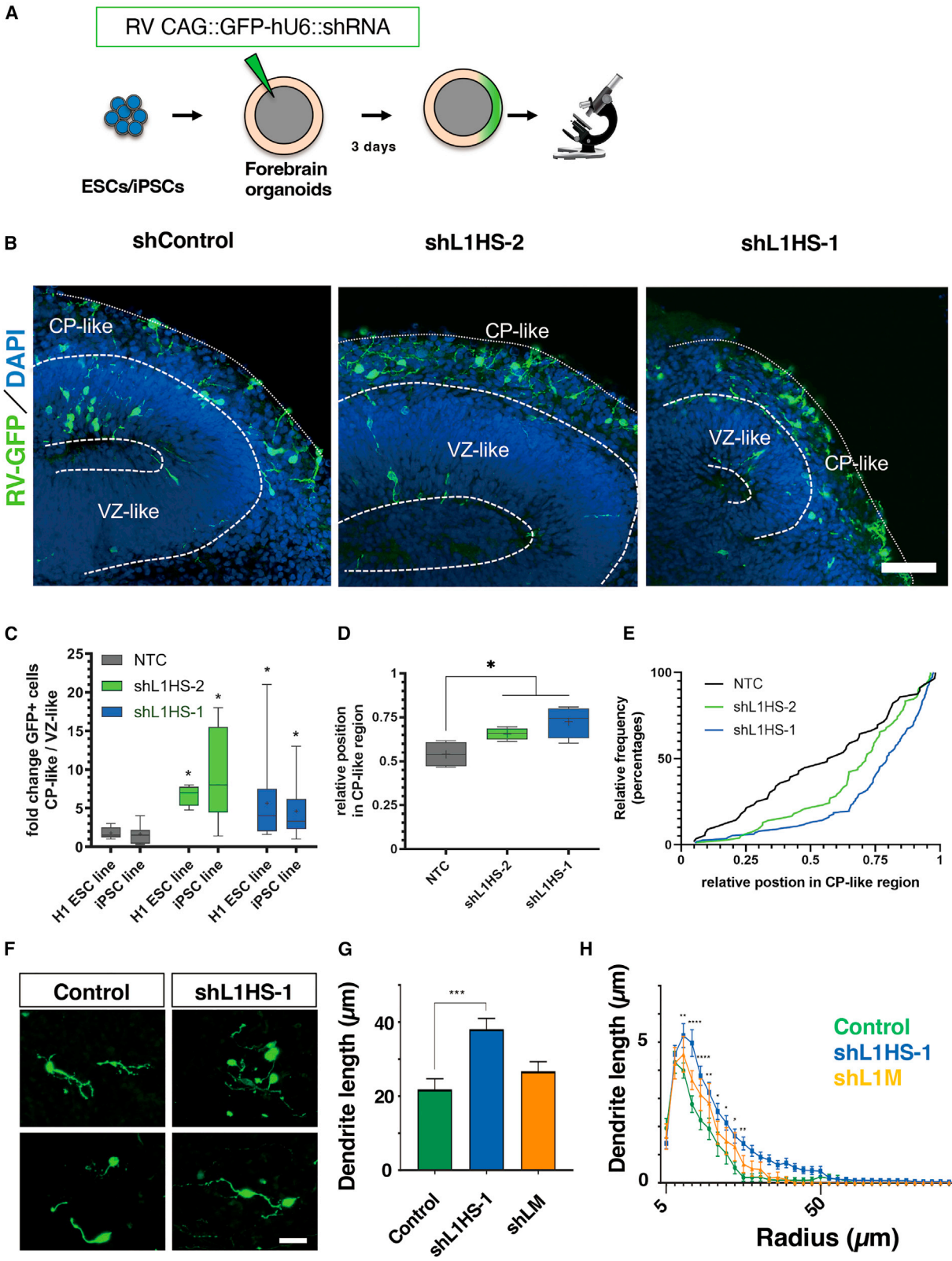

(legend on next page)

evolution, L1 RNA has been co-opted for functions in brain development. Understanding the molecular mechanisms underlying L1-dependent regulation in NPCs and differentiated neural cells will further elucidate how repetitive elements contribute to brain development, brain evolution, and the process of neoteny.

Limitations of the study

To address the roles of L1s in the regulation of NPCs, the study used a knockdown strategy with several shRNAs and L1 rescue experiments to verify the specificity of the effects derived from L1 manipulation. Despite these efforts, it still remains possible that the observed phenotype contains an off-target effect of shRNA. Therefore, future work should address the same questions using different methodologies to complement the findings from this study. While some mechanisms have elucidated for the effects of L1s in brain development, additional mechanisms need to be discovered to better understand these observed phenomena.

STAR★METHODS

Detailed methods are provided in the online version of this paper and include the following:

- KEY RESOURCES TABLE
- RESOURCES AVAILABILITY
  - Lead contact
  - Materials availability
  - Data and code availability
- EXPERIMENTAL MODEL AND STUDY PARTICIPANT DETAILS
  - Cell culture
  - Animals
  - Forebrain organoid culture
  - Plasmids
- METHOD DETAILS
  - qRT-PCR
  - *In utero* electroporation
  - Immunohistochemistry
  - Antibody generation anti-mouse LINE1-ORF1
  - Immunocytochemistry
  - ChIRP-qPCR
  - RNA sequencing and analyses
  - Forebrain organoid electroporation
  - Quantification of neural migration in forebrain organoids
  - Microscopy
  - 3D morphological analysis and cell counting
- QUANTIFICATION AND STATISTICAL ANALYSIS

SUPPLEMENTAL INFORMATION

Supplemental information can be found online at https://doi.org/10.1016/j.celrep.2024.113774.

ACKNOWLEDGMENTS

The authors thank M.L. Gage for critical reading of the manuscript; L. Moore, D. Julian, W. Schwind, L. Wallace, Dr. T.S. Sabedot, Dr. P. Hsu, and Dr. S. Konermann for technical assistance and discussions; and K. Diffenderfer and the Salk STEM Core Facility for technical support. We are also grateful to all members of the EMBL Protein Expression and Purification Core Facility for their support and help with the production and purification of antibodies anti-LINE1-ORF1, especially Kim Remans. The graphical abstract was made with BioRender. This work was supported by NIH U01 MH106882, NIH U01 MH114030, the AHA-Allen Initiative award 19PABH134610000, the Paul G. Allen Family Foundation, NIA Aging P01 grant AG051449, the Robert and Mary Jane Engman Foundation, the Stem Cell Core Facility and the Biophotonic Core Facility of the Salk Institute with funding from NIH-NCI CCSG (P30 CA014195), Takeda Pharmaceutical International, the JPB Foundation, a JSPS fellowship for research abroad (T.T.), a fellowship from the Paul F. Glenn Center for Biology of Aging Research (T.T.), Schram Foundation T0287/42406/2023 (T.T), DZNE (T.T), NIH F32 MH102983 (T.A.B), a National Alliance for Research on Schizophrenia and Depression Young Investigator Award (T.A.B.), and EMBL (M.B.).

AUTHOR CONTRIBUTIONS

T.T., T.A.B., S.T.S., and F.H.G. designed the experiments and wrote the manuscript. T.T., T.A.B., S.T.S., M.S.K., S.B.L., M.P., M.E.H., A.A.M., A.H.M., I.S.G., S.L.P., and N.N. performed the experiments and analyzed the data. M.B. provided resources. J.T.W., S.G., L.M., H.Y., C.L., and E.S. helped to analyze the data.

Figure 5. L1s regulate neural differentiation in human forebrain organoids

(A) A schema of the retroviral labeling procedure used to manipulate the levels of L1 in RGLs of forebrain organoids.

(B) Representative confocal images of VZ-like regions of retrovirally labeled RGL-derived cells that are migrating into the developing cortical plate of forebrain organoids. Sections were stained with anti-GFP (green) and DAPI. Scale bar, 50 μm.

(C) Fold change of retrovirally labeled RGLs 3 days post infection (dpi) observed in CP-like over VZ-like regions. Mann-Whitney U test, *$p < 0.05$. Boxplots with whiskers indicate minimum to maximum values, with box limits for 25th to 75th percentiles, and a centerline for the median.

(D) Relative normalized position of GFP-positive migratory cells within the evolving cortical plate of forebrain organoids. Mann-Whitney U test, *$p < 0.05$. Boxplots with whiskers indicate minimum to maximum values, with box limits for 25th to 75th percentiles, and a centerline for the median.

(E) Distribution of GFP-positive cells in the CP-like structures. Kolmogorov-Smirnov test, NTC (non-targeting control) vs. shL1HS-2: $p = 0.0177$, NTC vs. shL1HS-1: $p < 0.0001$.

(C–E) $N_{NTC} = 56$ cells (from n = 4 independent organoids; 2 organoids per iPSC, 2 organoids per ESC line), $N_{shL1HS-2} = 78$ cells (from n = 4 independent organoids; 2 organoids per iPSC, 2 organoids per ESC line), and $Ns_{hL1HS-1} = 113$ cells (from n = 4 independent organoids; 2 organoids per iPSC, 2 organoids per ESC line).

(F) Representative images of electroporated cells in the CP-like layer 2 weeks after the electroporation of shRNA plasmids. Scale bar, 25 μm.

(G) Quantification of dendritic length of electroporated cells. Data are presented as mean ± SEM. Mann-Whitney test, ***$p = 0.0019$.

(H) Sholl analysis for dendritic complexity of neurons in human cortical organoids. Two-way ANOVA followed by Holm-Sidak's multiple comparisons test, ***$p < 0.001$, **$p < 0.01$, and *$p < 0.05$. $N_{NTC} = 29$ cells (from n = 2 independent organoids), $N_{shL1HS-2} = 69$ cells (from n = 2 independent organoids), and $N_{shL1M} = 17$ cells (from n = 2 independent organoids).

Data are presented as mean ± SEM.

DECLARATION OF INTERESTS

The authors declare no competing interests.

Received: November 12, 2022
Revised: November 30, 2023
Accepted: January 24, 2024
Published: February 13, 2024

REFERENCES

1. Han, J.S., Szak, S.T., and Boeke, J.D. (2004). Transcriptional disruption by the L1 retrotransposon and implications for mammalian transcriptomes. Nature *429*, 268–274. https://doi.org/10.1038/nature02536.
2. Denli, A.M., Narvaiza, I., Kerman, B.E., Pena, M., Benner, C., Marchetto, M.C.N., Diedrich, J.K., Aslanian, A., Ma, J., Moresco, J.J., et al. (2015). Primate-specific ORF0 contributes to retrotransposon-mediated diversity. Cell *163*, 583–593. https://doi.org/10.1016/j.cell.2015.09.025.
3. Gasior, S.L., Wakeman, T.P., Xu, B., and Deininger, P.L. (2006). The human LINE-1 retrotransposon creates DNA double-strand breaks. J. Mol. Biol. *357*, 1383–1393. https://doi.org/10.1016/j.jmb.2006.01.089.
4. Pascarella, G., Hon, C.C., Hashimoto, K., Busch, A., Luginbühl, J., Parr, C., Hin Yip, W., Abe, K., Kratz, A., Bonetti, A., et al. (2022). Recombination of repeat elements generates somatic complexity in human genomes. Cell *185*, 3025–3040.e6. https://doi.org/10.1016/j.cell.2022.06.032.
5. Jönsson, M.E., Ludvik Brattås, P., Gustafsson, C., Petri, R., Yudovich, D., Pircs, K., Verschuere, S., Madsen, S., Hansson, J., Larsson, J., et al. (2019). Activation of neuronal genes via LINE-1 elements upon global DNA demethylation in human neural progenitors. Nat. Commun. *10*, 3182. https://doi.org/10.1038/s41467-019-11150-8.
6. De Cecco, M., Ito, T., Petrashen, A.P., Elias, A.E., Skvir, N.J., Criscione, S.W., Caligiana, A., Brocculi, G., Adney, E.M., Boeke, J.D., et al. (2019). L1 drives IFN in senescent cells and promotes age-associated inflammation. Nature *566*, 73–78. https://doi.org/10.1038/s41586-018-0784-9.
7. Simon, M., Van Meter, M., Ablaeva, J., Ke, Z., Gonzalez, R.S., Taguchi, T., De Cecco, M., Leonova, K.I., Kogan, V., Helfand, S.L., et al. (2019). LINE1 Derepression in Aged Wild-Type and SIRT6-Deficient Mice Drives Inflammation. Cell Metabol. *29*, 871–885.e5. https://doi.org/10.1016/j.cmet.2019.02.014.
8. Della Valle, F., Reddy, P., Yamamoto, M., Liu, P., Saera-Vila, A., Bensaddek, D., Zhang, H., Prieto Martinez, J., Abassi, L., Celii, M., et al. (2022). LINE-1 RNA causes heterochromatin erosion and is a target for amelioration of senescent phenotypes in progeroid syndromes. Sci. Transl. Med. *14*, eabl6057. https://doi.org/10.1126/scitranslmed.abl6057.
9. Muotri, A.R., Chu, V.T., Marchetto, M.C.N., Deng, W., Moran, J.V., and Gage, F.H. (2005). Somatic mosaicism in neuronal precursor cells mediated by L1 retrotransposition. Nature *435*, 903–910. https://doi.org/10.1038/nature03663.
10. Sookdeo, A., Hepp, C.M., McClure, M.A., and Boissinot, S. (2013). Revisiting the evolution of mouse LINE-1 in the genomic era. Mobile DNA *4*, 3. https://doi.org/10.1186/1759-8753-4-3.
11. Naito, Y., Yoshimura, J., Morishita, S., and Ui-Tei, K. (2009). siDirect 2.0: updated software for designing functional siRNA with reduced seed-dependent off-target effect. BMC Bioinf. *10*, 392. https://doi.org/10.1186/1471-2105-10-392.
12. Bonev, B., Mendelson Cohen, N., Szabo, Q., Fritsch, L., Papadopoulos, G.L., Lubling, Y., Xu, X., Lv, X., Hugnot, J.P., Tanay, A., and Cavalli, G. (2017). Multiscale 3D Genome Rewiring during Mouse Neural Development. Cell *171*, 557–572.e24. https://doi.org/10.1016/j.cell.2017.09.043.
13. McKerrow, W., and Fenyö, D. (2020). L1EM: a tool for accurate locus specific LINE-1 RNA quantification. Bioinformatics *36*, 1167–1173. https://doi.org/10.1093/bioinformatics/btz724.
14. Bedrosian, T.A., Quayle, C., Novaresi, N., and Gage, F.H. (2018). Early life experience drives structural variation of neural genomes in mice. Science *359*, 1395–1399. https://doi.org/10.1126/science.aah3378.
15. An, W., Han, J.S., Wheelan, S.J., Davis, E.S., Coombes, C.E., Ye, P., Triplett, C., and Boeke, J.D. (2006). Active retrotransposition by a synthetic L1 element in mice. Proc. Natl. Acad. Sci. USA *103*, 18662–18667. https://doi.org/10.1073/pnas.0605300103.
16. Tabata, H., and Nakajima, K. (2001). Efficient in utero gene transfer system to the developing mouse brain using electroporation: visualization of neuronal migration in the developing cortex. Neuroscience *103*, 865–872.
17. Saito, T., and Nakatsuji, N. (2001). Efficient gene transfer into the embryonic mouse brain using in vivo electroporation. Dev. Biol. *240*, 237–246. https://doi.org/10.1006/dbio.2001.0439.
18. Sehara, K., Toda, T., Iwai, L., Wakimoto, M., Tanno, K., Matsubayashi, Y., and Kawasaki, H. (2010). Whisker-related axonal patterns and plasticity of layer 2/3 neurons in the mouse barrel cortex. J. Neurosci. *30*, 3082–3092.
19. Taverna, E., Götz, M., and Huttner, W.B. (2014). The cell biology of neurogenesis: toward an understanding of the development and evolution of the neocortex. Annu. Rev. Cell Dev. Biol. *30*, 465–502. https://doi.org/10.1146/annurev-cellbio-101011-155801.
20. Erwin, J.A., Marchetto, M.C., and Gage, F.H. (2014). Mobile DNA elements in the generation of diversity and complexity in the brain. Nat. Rev. Neurosci. *15*, 497–506. https://doi.org/10.1038/nrn3730.
21. Fietz, S.A., Lachmann, R., Brandl, H., Kircher, M., Samusik, N., Schröder, R., Lakshmanaperumal, N., Henry, I., Vogt, J., Riehn, A., et al. (2012). Transcriptomes of germinal zones of human and mouse fetal neocortex suggest a role of extracellular matrix in progenitor self-renewal. Proc. Natl. Acad. Sci. USA *109*, 11836–11841. https://doi.org/10.1073/pnas.1209647109.
22. Percharde, M., Lin, C.J., Yin, Y., Guan, J., Peixoto, G.A., Bulut-Karslioglu, A., Biechele, S., Huang, B., Shen, X., and Ramalho-Santos, M. (2018). A LINE1-Nucleolin Partnership Regulates Early Development and ESC Identity. Cell *174*, 391–405.e19. https://doi.org/10.1016/j.cell.2018.05.043.
23. Hoshiba, Y., Toda, T., Ebisu, H., Wakimoto, M., Yanagi, S., and Kawasaki, H. (2016). Sox11 Balances Dendritic Morphogenesis with Neuronal Migration in the Developing Cerebral Cortex. J. Neurosci. *36*, 5775–5784. https://doi.org/10.1523/JNEUROSCI.3250-15.2016.
24. Schafer, S.T., Paquola, A.C.M., Stern, S., Gosselin, D., Ku, M., Pena, M., Kuret, T.J.M., Liyanage, M., Mansour, A.A., Jaeger, B.N., et al. (2019). Pathological priming causes developmental gene network heterochronicity in autistic subject-derived neurons. Nat. Neurosci. *22*, 243–255. https://doi.org/10.1038/s41593-018-0295-x.
25. Lancaster, M.A., Renner, M., Martin, C.A., Wenzel, D., Bicknell, L.S., Hurles, M.E., Homfray, T., Penninger, J.M., Jackson, A.P., and Knoblich, J.A. (2013). Cerebral organoids model human brain development and microcephaly. Nature *501*, 373–379. https://doi.org/10.1038/nature12517.
26. Sun, W., Samimi, H., Gamez, M., Zare, H., and Frost, B. (2018). Pathogenic tau-induced piRNA depletion promotes neuronal death through transposable element dysregulation in neurodegenerative tauopathies. Nat. Neurosci. *21*, 1038–1048. https://doi.org/10.1038/s41593-018-0194-1.
27. Evrony, G.D., Cai, X., Lee, E., Hills, L.B., Elhosary, P.C., Lehmann, H.S., Parker, J.J., Atabay, K.D., Gilmore, E.C., Poduri, A., et al. (2012). Single-neuron sequencing analysis of L1 retrotransposition and somatic mutation in the human brain. Cell *151*, 483–496. https://doi.org/10.1016/j.cell.2012.09.035.
28. Upton, K.R., Gerhardt, D.J., Jesuadian, J.S., Richardson, S.R., Sánchez-Luque, F.J., Bodea, G.O., Ewing, A.D., Salvador-Palomeque, C., van der Knaap, M.S., Brennan, P.M., et al. (2015). Ubiquitous L1 mosaicism in hippocampal neurons. Cell *161*, 228–239. https://doi.org/10.1016/j.cell.2015.03.026.
29. Erwin, J.A., Paquola, A.C.M., Singer, T., Gallina, I., Novotny, M., Quayle, C., Bedrosian, T.A., Alves, F.I.A., Butcher, C.R., Herdy, J.R., et al. (2016). L1-associated genomic regions are deleted in somatic cells of

the healthy human brain. Nat. Neurosci. *19*, 1583–1591. https://doi.org/10.1038/nn.4388.

30. Sanchez-Luque, F.J., Kempen, M.J.H.C., Gerdes, P., Vargas-Landin, D.B., Richardson, S.R., Troskie, R.L., Jesuadian, J.S., Cheetham, S.W., Carreira, P.E., Salvador-Palomeque, C., et al. (2019). LINE-1 Evasion of Epigenetic Repression in Humans. Mol. Cell *75*, 590–604.e12. https://doi.org/10.1016/j.molcel.2019.05.024.
31. Gould, S.J. (1977). Ontogeny and Phylogeny (Harvard Univ Press).
32. Carroll, S.B. (2003). Genetics and the making of Homo sapiens. Nature *422*, 849–857. https://doi.org/10.1038/nature01495.
33. Linker, S.B., Narvaiza, I., Hsu, J.Y., Wang, M., Qiu, F., Mendes, A.P.D., Oefner, R., Kottilil, K., Sharma, A., Randolph-Moore, L., et al. (2022). Human-specific regulation of neural maturation identified by cross-primate transcriptomics. Curr. Biol. *32*, 4797–4807.e5. https://doi.org/10.1016/j.cub.2022.09.028.
34. Jachowicz, J.W., Bing, X., Pontabry, J., Bošković, A., Rando, O.J., and Torres-Padilla, M.E. (2017). LINE-1 activation after fertilization regulates global chromatin accessibility in the early mouse embryo. Nat. Genet. *49*, 1502–1510. https://doi.org/10.1038/ng.3945.
35. Mangoni, D., Simi, A., Lau, P., Armaos, A., Ansaloni, F., Codino, A., Damiani, D., Floreani, L., Di Carlo, V., Vozzi, D., et al. (2023). LINE-1 regulates cortical development by acting as long non-coding RNAs. Nat. Commun. *14*, 4974. https://doi.org/10.1038/s41467-023-40743-7.
36. Burke, E.E., Chenoweth, J.G., Shin, J.H., Collado-Torres, L., Kim, S.K., Micali, N., Wang, Y., Colantuoni, C., Straub, R.E., Hoeppner, D.J., et al. (2020). Dissecting transcriptomic signatures of neuronal differentiation and maturation using iPSCs. Nat. Commun. *11*, 462. https://doi.org/10.1038/s41467-019-14266-z.
37. Garza, R., Atacho, D., Adami, A., Gerdes, P., Vinod, M., Hsieh, P., Karlsson, O., Horvath, V., Johansson, P.A., Pandiloski, N., et al. (2023). L1 retrotransposons drive human neuronal transcriptome complexity and functional diversification. Preprint at bioRxiv. https://doi.org/10.1101/2023.03.04.531072.
38. Schafer, S.T., Han, J., Pena, M., von Bohlen Und Halbach, O., Peters, J., and Gage, F.H. (2015). The Wnt adaptor protein ATP6AP2 regulates multiple stages of adult hippocampal neurogenesis. J. Neurosci. *35*, 4983–4998. https://doi.org/10.1523/JNEUROSCI.4130-14.2015.
39. Bonev, B., Mendelson Cohen, N., Szabo, Q., Fritsch, L., Papadopoulos, G.L., Lubling, Y., Xu, X., Lv, X., Hugnot, J.-P., Tanay, A., and Cavalli, G. (2017). Multiscale 3D genome rewiring during mouse neural development. Cell *171* (3), 557–572.
40. Schindelin, J., Arganda-Carreras, I., Frise, E., Kaynig, V., Longair, M., Pietzsch, T., Preibisch, S., Rueden, C., Saalfeld, S., Schmid, B., et al. (2012). Fiji: an open-source platform for biological-image analysis. Nat. Methods *9*, 676–682. https://doi.org/10.1038/nmeth.2019.
41. Robinson, M.D., McCarthy, D.J., and Smyth, G.K. (2010). edgeR: a Bioconductor package for differential expression analysis of digital gene expression data. Bioinformatics *26*, 139–140. https://doi.org/10.1093/bioinformatics/btp616.
42. Cox, M.P., Peterson, D.A., and Biggs, P.J. (2010). SolexaQA: At-a-glance quality assessment of Illumina second-generation sequencing data. BMC Bioinf. *11*, 485. https://doi.org/10.1186/1471-2105-11-485.
43. Langmead, B., and Salzberg, S.L. (2012). Fast gapped-read alignment with Bowtie 2. Nat Methods *9*, 359–359.
44. Heinz, S., Benner, C., Spann, N., Bertolino, E., Lin, Y.C., Laslo, P., Cheng, J.X., Murre, C., Singh, H., and Glass, C.K. (2010). Simple combinations of lineage-determining transcription factors prime cis-regulatory elements required for macrophage and B cell identities. Mol. Cell *38*, 576–589. https://doi.org/10.1016/j.molcel.2010.05.004.
45. Ray, J., and Gage, F.H. (2006). Differential properties of adult rat and mouse brain-derived neural stem/progenitor cells. Mol. Cell. Neurosci. *31*, 560–573. https://doi.org/10.1016/j.mcn.2005.11.010.
46. Xie, Y., Rosser, J.M., Thompson, T.L., Boeke, J.D., and An, W. (2011). Characterization of L1 retrotransposition with high-throughput dual-luciferase assays. Nucleic Acids Res. *39*, e16. https://doi.org/10.1093/nar/gkq1076.
47. Toda, T., Homma, D., Tokuoka, H., Hayakawa, I., Sugimoto, Y., Ichinose, H., and Kawasaki, H. (2013). Birth regulates the initiation of sensory map formation through serotonin signaling. Dev. Cell *27*, 32–46.
48. Toda, T., Hsu, J.Y., Linker, S.B., Hu, L., Schafer, S.T., Mertens, J., Jacinto, F.V., Hetzer, M.W., and Gage, F.H. (2017). Nup153 Interacts with Sox2 to Enable Bimodal Gene Regulation and Maintenance of Neural Progenitor Cells. Cell Stem Cell *21*, 618–634.e7. https://doi.org/10.1016/j.stem.2017.08.012.
49. Li, B., and Dewey, C.N. (2011). RSEM: accurate transcript quantification from RNA-Seq data with or without a reference genome. BMC Bioinf. *12*, 323. https://doi.org/10.1186/1471-2105-12-323.
50. Bao, W., Kojima, K.K., and Kohany, O. (2015). Repbase Update, a database of repetitive elements in eukaryotic genomes *6*, 11. https://doi.org/10.1186/s13100-015-0041-9.

STAR★METHODS

KEY RESOURCES TABLE

REAGENT or RESOURCE	SOURCE	IDENTIFIER
Antibodies		
Rabbit polyclonal anti-Sox2	Cell signaling	#2748; RRID: AB_823640
Goat polyclonal anti-Sox2	Santa Cruz	sc17320; RRID: AB_2286684
Goat polyclonal anti-DCX	Santa Cruz	Sc-8066; RRID: AB_2088494
Chick polyclonal anti-GFP	Aves Lab	GFP-1020; RRID: AB_10000240
Rabbit polyclonal anti-S100β	Swant	37A; RRID: AB_2315305
Mouse monoclonal anti-Ki67	BD Pharminger	550609; RRID: AB_393778
Mouse anti-Nestin	Santa Cruz	347580
Chicken anti-Map2	Abcam	AP20; RRID: AB_1824237
Rabbit anti-Tuj1	BioLegend	MRB-435P; RRID: AB663339
Rabbit anti-GFAP	Dako	Z0334; RRID: AB_10013382
Rabbit polyclonal anti-GFP	LifeTechnology	A11122; RRID: AB_2307355
Rabbit anti-mouse Orf1	This study	N/A
Mouse anti-human ORF1	Millopore	4H1; RRID: AB_2941775
Rat anti-Ctip2	Abcam	25B6: RRID: AB_2064130
Bacterial and virus strains		
Retrovirus; pCAG07-GFP-hU6-shRNA	Schafer et al.[38]	N/A
Chemicals, peptides, recombinant proteins and reagents		
FGF2	PeproTech	100-18A
EGF	PeproTech	10014
Retinoic acid	Sigma	R-2625
Forskolin	Sigma	F-6886
Laminin	Invitrogen	A256075
Bovine albumin serum (BSA)	Fisher Scientific	BP1600-1
Fetal bovine serum (FBS)		1500–500
ProLong® Gold Antifade Mountant	ThermoFisher	P36934
TRIzol® LS Reagent	ThermoFisher	10296028
B-27 supplement	Invitrogen	12587010
DMEM/F-12 L-Glutamine media	ThermoFisher	11320–033
Heparin	Sigma	H2149
PEI	Polysciences Inc	#23966
Puromycin	Gibco	A11138-03
Rock inhibitor	Stem Cell Technologies	72308
20% Knockout Serum Replacer	Thermo Fischer	Cat# 10828028
Non-essential Amino Acids	Thermo Fischer	Cat# 1114005
collagenase Type IV	Gibco	Cat# 17104-019
2-mercaptoethanol	Thermo Fischer	Cat# 21985023
GlutaMAX	Thermo Fischer	Cat# 35050061
ROCK inhibitor Y-27632	Tocris	Cat# 1254
Dorsomorphin	Cayman Chemicals	N/A
SB-431542	Tocris	Cat# 1614
Cultrex Reduced Growth Factor Basement Membrane Extract	R&D	Cat# 3433-005-01
Insulin	Millipore	Cat# I9278
A-083	Stemgent	Cat# 04-0014-10

(*Continued on next page*)

Continued

REAGENT or RESOURCE	SOURCE	IDENTIFIER
Critical commercial assays		
Nucleofector Kit for mouse neural stem cells	Lonza	VPG-1004
Deposited data		
RNA-seq data for the knockout of L1	This study	GEO: GSE217643
Mouse NPC and neuron RNA seq data	Bonev et al.[39]	GEO: GSE96107
Human iPSC to neurons RNA-seq data	Burke et al.[36]	SRA: PRJNA596331
Experimental models: Cell lines		
Mouse cortical neural progenitors	This study	N/A
Human iPSC and ESC lines	Schafer et al.[24]	Cove 3-1 iPSC Cent 3–6 iPSC
Experimental models: Organisms/strains		
Mouse: C57BL/6	N/A	Harlan/Evigo
Oligonucleotides		
Please see Table S1		N/A
Recombinant DNA		
pWA125-L1	An et al.[15]	NA
pWA125-mL1	An et al.[15]	N/A
Software and algorithms		
Fiji/ImageJ	Schindelin et al.[40]	https://fiji.sc
R	Robinson et al.[41]	https://www.r-project.org
SolexaQA++	Cox et al.[42]	N/A
Bowtie2	Langmead and Salzberg[43]	http://bowtie-bio.sourceforge.net/bowtie2/index.shtml
Homer	Heinz et al.[44]	N/A
Rstudio3		N/A
siDirect 2.0	Naito et al.[11]	N/A
L1EM	McKerrow et al.[13]	N/A

RESOURCES AVAILABILITY

Lead contact

Further information and Requests for resources and reagents should be directed to the lead contact, Fred H. Gage (gage@salk.edu).

Materials availability

All biological materials used in this study are available from the lead contact upon request or from commercial sources.

Data and code availability

The RNA sequencing data have been deposited at GEO (GSE217643), and publicly available.

This paper does not report original code.

All data needed to evaluate the conclusions in the paper are present in the paper and/or the Supplemental Information. Any additional information required to reanalyze the data reported in this paper is available from the lead contact upon request.

EXPERIMENTAL MODEL AND STUDY PARTICIPANT DETAILS

Cell culture

The mouse NPCs isolated from C57BL/6 mice were cultured as described previously.[45] NPCs were cultured in DMEM/F-12 supplemented with N2 and B27 (Invitrogen) in the presence of FGF2 (10 ng/mL), EGF (10 ng/mL), laminin (1 μg/ml) and heparin (5 μg/mL). NPCs were passaged every two to three days and media was changed. HEK293T cells were cultured in IMDM supplemented with 5% fetal bovine serum at 37°C. For differentiation, EGF was withdrawn from the proliferating media, and cells were fixed with 4% PFA/PBS 3 days after the removal of EGF. For human cells, this study's protocol was approved by Salk Institute's IRB Committee (FWA 00005316) and the Embryonic Stem Cell Research and Oversight Committee. The Salk Institute is committed to protecting the

rights and welfare of human research participants and ensures compliance with all applicable ethical and legal requirements. After a complete description of the study, written informed consent was provided by the parents of the human participants.

Animals

All animal procedures were performed in accordance with protocols approved by the Animal Care and Use Committee of The Salk Institute for Biological Studies. Experiments were conducted in accordance with the National Institutes of Health's Guide for the Care and Use of Laboratory Animals and the US Public Health Service's Policy on Humane Care and Use of Laboratory Animals. C57BL/6 mice were purchased from Harlan/Envigo and were bred in the Salk animal facility. Animals were housed under constant temperature and humidity on a 12-h light-dark cycle with free access to food and water.

Forebrain organoid culture

Forebrain organoids were generated as described previously.[24] Briefly, human iPSC or ESC colonies were detached with collagenase Type IV (Gibco) and transferred to an Ultra-Low attachment 10-cm plate (Corning Costar) containing hPSC medium that consisted of DMEM:F12 (Invitrogen), 20% Knockout Serum Replacer (Gibco), 1x Non-essential Amino Acids (Invitrogen), 1x β-mercaptoethanol (Gibco), 1x GlutaMAX (Invitrogen), 10 ng/mL FGF-2 (Peprotech) and ROCK inhibitor Y27632 (10 μM). One day later, the medium was replaced with induction medium containing hPSC media, 2 μM dorsomorphin (Cayman Chemical) and 2 μM A-083 (Stemgent) without FGF-2. Five days later, the media were replaced with neural induction medium, consisting of DMEM:F12 (Invitrogen), 1x N2 Supplement (Invitrogen), 1x Non-essential Amino Acids (Invitrogen), 1x GlutaMAX (Invitrogen), 10 μg/mL Heparin (Sigma), 1x Penicillin/Streptomycin (Gibco), 10 μM CHIR99021 (Cayman) and 1 μM SB-431542 (Stemgent). Seven days after induction, organoids were embedded in 20 μL Matrigel (Trevigen) droplets and continued to grow for an additional week in 6-cm Ultra-Low attachment plates (Corning Costar). From day 14 onwards, organoids were cultured in differentiation medium comprising DMEM:F12 (Invitrogen), 1x N2 and B27 Supplements (Invitrogen), 1x Non-essential Amino Acids (Invitrogen), 1xGlutaMAX (Invitrogen), 1x β-Mercaptoethanol (Gibco), 1x Penicillin/Streptomycin (Gibco) and 2.5 μg mL/1 Insulin (Sigma), and were transferred to an orbital shaker (65–80 rpm). At day 20, residual Matrigel was removed and media changes were performed every two to three days using the aforementioned differentiation medium.

Plasmids

For knockdown experiments, shRNAs targeting mouse or human L1s were designed using siDirect2.0.[11] siRNA sequences were designed to target the active mouse L1 families (L1MdA_1, L1MdTf_I and L1MdGf_I) as well as the inactive mouse L1 families (L1 MdV, L1MdFanc_I, L1Mur1) (Table S1). shRNAs were cloned into a construct containing a chicken β-actin (CAG)-driven green fluorescent protein (GFP) and an hU6 promoter driving expression of shRNAs[38] or pLKO1 vector for puromycin selection. shRNA targeting the active human L1 (L1HS) and the inactive human L1 (L1M) were similarly constructed. Knockdown efficiencies of L1 expression were confirmed by qRT-PCR following transfection into mouse NPCs and HEK293T. To exogenously express L1, codon-optimized mouse full-length WT L1 (FL-L1; pWA-125) and mutated-L1 (mL1; pWA-126) with its endogenous 5′UTR, an upstream CMV promoter and a retrotransposition-dependent GFP expression cassette were used.[46] Plasmids were purified using the PureLink HiPure Plasmid Filter Maxiprep Kit (Invitrogen). Before *in utero* electroporation procedures, plasmid DNA was diluted to 1 mg/mL in 1x PBS, and Fast Green solution was added to a final concentration of 0.05% to monitor the injection.

METHOD DETAILS

qRT-PCR

Total RNA was extracted using RNeasy Plus Mini kit (Qiagen) and extracted RNA was treated by TURBO DNase (Ambion). cDNA was reverse transcribed from RNA using a QuantiTect Reverse Transcription Kit (Qiagen) with gDNA wipeout treatment. Quantitative RT-PCR was performed using the C1000Touch cycler (Bio-Rad) for Sybr Green (HEK293T and mouse NPCs) or ABI 7900 instrument (Applied Biosystems) for Taqman (mouse NPCs). Real time qPCR with Taqman assay was performed in duplex with Gapdh (Mm99999915_g1, Life Technologies) as a reference gene; cycling conditions were 50°C for 2 min and 95°C for 10 min, followed by 40 cycles of 95°C for 15 s and 60°C for 1 min. No template and no reverse transcription (RT) controls were included. Expression levels were determined relative to Gapdh or β-actin using the delta delta Ct method. siRNA sequence and primers used for qRT-PCR are listed in Table S1.

In utero electroporation

In utero electroporation was performed as previously described with slight modifications.[18] Briefly, pregnant C57BL/6 mice were anesthetized with isoflurane (2.5–3%), and the uterine horns were exposed. Approximately 1–2 μL of DNA solution (2 mg/mL) was injected into the lateral ventricle of the brains of embryos at E15.5 using a pulled glass micropipette. Each embryo was held between tweezer-type electrodes with an electroporator CUY21EDIT (BEX, 0.5 cm puddle type electrode, 35 V, 50 ms duration, 950 ms intervals, 5 pulses). Care was taken to quickly place embryos back into the abdominal cavity to avoid excessive temperature loss. The wall and skin of the abdominal cavity were sutured. Dams were given an injection of buprenorphine and recovered in a home cage.

Immunohistochemistry

Dams were deeply anesthetized with ketamine/xylazine/acepromazine. Brains from embryos were dissected out and fixed in 4% paraformaldehyde (PFA) in PBS, pH 7.4, overnight at 4°C and then transferred into 30% sucrose solution for cryoprotection. Fifty μm-thick coronal sections were obtained using a cryostat (Leica) and were subjected to immunohistochemistry as previously described.[47] Secondary antibodies were all obtained from Jackson Immunoresearch.

Antibody generation anti-mouse LINE1-ORF1

The DNA sequence encoding murine LINE1-ORF1 (Uniprot P11260) was codon-optimized for *E. coli*, synthetized (IDT) and subcloned in the pETM11-SUMO3 expression vector (EMBL). The pETM11-SUMO3-LINE1-ORF1 expression plasmid was freshly transformed into *E. coli* BL21-CodonPlus(DE3)-RIL cells. Precultures were grown at 37°C in LB medium supplemented with 30 μg/mL Kanamycin and 34 μg/mL Chloramphenicol and used to inoculate the large-scale expression cultures. Ten mL preculture was added to 1 L of TB-FB medium supplemented with 1.5% lactose, 30 μg/mL Kanamycin and 34 μg/mL Chloramphenicol. The *E. coli* cultures were grown overnight at 25°C and harvested by centrifugation (30 min, 5000 *g*, 4°C). The cell pellets were flash-frozen in liquid nitrogen and stored at −80°C until the start of the protein purification.

All steps of the protein purification process were performed at 4°C and samples were stored on ice throughout the whole workflow. The cell pellet was resuspended in cold lysis buffer (50 mM Tris-HCl pH 8.0, 250 mM NaCl, 20 mM imidazole) supplemented with 1 μg/mL DNaseI, 5 mM $MgCl_2$ and EDTA-free cOmplete protease inhibitors (Roche). After resuspension, 1 mg/mL lysozyme was added and the mixture was incubated for 30 min at 4°C. The cells were lysed by 3 passages through a microfluidizer device, followed by centrifugation (30 min, 140000 x *g*, 4°C). The cleared lysate was loaded onto a 5 mL Protino Ni-NTA column (Macherey-Nagel) pre-equilibrated with 50 mM Tris-HCl pH 8.0, 250 mM NaCl, 20 mM imidazole. After loading, the Ni-NTA column was washed with equilibration buffer and eluted with equilibration buffer supplemented with 300 mM imidazole. The elution samples were analyzed by SDS-PAGE and the fractions containing the His_6-SUMO3-LINE1-ORF1 fusion protein were pooled. His_6-tagged SenP2 protease was added to the pooled elution fractions to remove the His_6-SUMO3 fusion tag and the entire sample was dialyzed overnight against 50 mM Tris-HCl pH 8.0, 250 mM NaCl, 20 mM imidazole at 4°C. The next day, the dialyzed sample was loaded again onto a 5 mL Protino Ni-NTA column (Macherey-Nagel). Untagged LINE1-ORF1 protein was collected in the flow-through and dialyzed overnight against 50 mM Tris-HCl pH 7.0, 50 mM NaCl. The dialyzed LINE1-ORF1 sample was loaded onto a 5 mL HiTrap Q HP column (Cytiva) pre-equilibrated with IEX buffer (50 mM Tris-HCl pH 7.0, 50 mM NaCl). After washing with IEX equilibration buffer, the HiTrap Q HP column was eluted in a gradient going from 50 mM NaCl to 1 M NaCl over 12 column volumes. The elution fractions containing LINE1-ORF1 were pooled and concentrated to ∼4.4 mg/mL. Aliquots containing the LINE1-ORF1 protein (in 50 mM Tris-HCl pH 7.0, 600 mM NaCl) were flash-frozen and stored at −80°C. Identity and intactness of the LINE1-ORF1 protein were verified by mass spectrometry by the EMBL Proteomics Core Facility.

Polyclonal antibodies against the purified LINE1-ORF1 protein were raised in a New Zealand White rabbit at the EMBL Laboratory Animal Resources facility. After the immunization process, the rabbit was sacrificed by exsanguination. The serum was isolated from the final bleed sample and used for antibody purification. Purified LINE1-ORF1 protein was covalently coupled to NHS-activated agarose beads (Pierce) according to the manufacturer's specifications. The serum was diluted 1:1 in PBS and incubated overnight with the LINE1-ORF1 resin pre-equilibrated in PBS. After overnight incubation, the resin was washed with PBS and the LINE1-ORF1-specific antibodies were eluted with 100 mM Glycin pH 2.4, 150 mM NaCl. The elution fractions were immediately neutralized with 1 M Tris pH 8.5. The elution fractions were analyzed by SDS-PAGE and the fractions containing antibodies were pooled.

Immunocytochemistry

Immunocytochemistry was performed as described previously, with slight modifications.[48] Briefly, cultured cells were fixed with 4% PFA for 10 min at room temperature followed by three washes in PBS and were then permeabilized with 0.1% Triton X-100 in TBS, blocked with 3% horse serum and incubated with primary antibody overnight.

ChIRP-qPCR

ChIRP experiments were performed using two sets of non-overlapping biotinylated probes (even and odd sets) designed for the mouse L1spa element.[22] Mouse NPCs were differentiated and harvested at days 0 and 3. ChIRP was performed using a Magna ChIRP RNA Interactome Kit (Millipore) according to manufacturer's instructions. Briefly, ∼1 x 10^7 cells were crosslinked in 1% glutaraldehyde for 10 min and then quenched with glycine. Cell pellets were washed, lysed, and then sonicated using a Bioruptor Pico (Diagenode) to shear cross-linked chromatin to ∼100–500 base pairs in length. Sheared chromatin was incubated overnight with biotinylated L1 probes (50 μM) at 37°C. A negative control reaction was incubated with LacZ probes. Hybridized RNA-chromatin complexes were captured on streptavidin magnetic beads and washed, and then DNA was eluted and purified using a MinElute PCR purification kit (Qiagen). Enrichments were analyzed by Sybr Green qPCR (ABI Step One Plus) and percent input was calculated using the delta Ct method. Primers for expected negative regions were used to assess background levels of enrichment (Gapdh, Actin, Rpl3-Tss, and IntChr11).

RNA sequencing and analyses

After the electroporation of shRNAs, GFP-positive cells were sorted directly into Trizol-LS (Invitrogen). RNA was isolated according to the manufacturer's instructions and digested with TURBO DNase (Life Technologies). RNA integrity numbers (RIN) were assessed

using the Agilent Tape Station before library preparation and RNA was amplified with SMARTseq2 protocol to read 5′-UTR of RNA and the Nextera XT kit was used for sample preparation. Libraries were sequenced paired-end 150 bp (PE150) using an Illumina NextSeq sequencer at the Next Generation Sequencing (NGS) core at the Salk Institute according to manufacturer's instructions (Illumina).

Reads were trimmed for quality and adapter sequence. To maintain only high-quality bases, reads were first trimmed using the dynamictrim function from SolexaQA++.[42] Template-switch oligo (TSO) sequences were removed using cutadapt and requiring that sequences with at least 30bp were retained for downstream counting. Trimmed reads were then aligned to the mouse genome using the rsem-calculate-expression function from RSEM.[49] Transcripts per million (TPM) were $\log_2 + 1$ normalized for visualization and differential expression calculations using a mixed effects model. To accommodate the mixed effect study design, the lmer function from the lme4 package was used for differential expression analysis in R version 3.6.1 with shL1s for active L1s as the fixed effect and the construct as the random effect. p-values were adjusted for multiple-testing using the p.adjust (method = "holm") function in R.

The genome-wide binding sites for each shRNA were computationally identified by searching for each sequence and its reverse complement, with one allowable mismatch, to the mm10 reference genome using the regular expression library (re) in python 3.6. Distances to the closest promoter were identified by intersecting shRNA binding sites with a bed file of complete gene lengths from RefSeq (transcription start to transcription stop). To predict the numbers of shRNA targeted L1 subfamilies, shRNA sequences were aligned to the L1 elements in the Repbase.[50] To quantify the expression levels of L1 elements and the effects of shRNAs on L1 expression globally, L1EM was used.[13]

Forebrain organoid electroporation

For electroporation, DNA solution (2 mg/mL) was injected into the ventricle of five-to eight-week-old forebrain organoids using a pulled glass micropipette. Each organoid was placed between tweezer-type electrodes with an electroporator BTX ECM830 (0.3 cm puddle type electrode, 35 V, 50 ms duration, 950 ms intervals, 5 pulses × 2 shot) in PBS. After electroporation, organoids were put back in differentiation medium for three days for migration analysis or 14 days for morphological analysis. Organoids were fixed in 4% PFA for 45 min and then transferred into 30% sucrose solution for cryoprotection. Twenty μm-thick sections were obtained using a cryostat (Leica) and subjected to immunohistochemistry as previously described.[24] A total of three or four forebrain organoids with 1–3 'VZ-like' regions per organoid were quantified for every condition.

Retrovirally labeled newborn neurons were analyzed in forebrain organoids at 3 dpi in regions that showed clearly defined VZ-like and CP-like structures. The migratory distance was assessed based on the relative position of GFP (RV-CAG::GFP) within CP-like regions and analyzed using Neurolucida version 11 (MBF Bioscience). In total, two lines (1 neurotypical iPSC line and one H1 ESC line) were analyzed with three to five organoid replicates per individual.

Quantification of neural migration in forebrain organoids

To normalize the thickness of VZ among rosettes, the thicknesses of VZ were normalized to 100%, and the distances of GFP-positive cells were measured from the ventricle using ImageJ. Distances of GFP-positive cells migrating into the CP were considered as 100% or more.

Microscopy

Fluorescence was detected using a Zeiss LSM 880. Images were acquired with 20x and 63x objectives and the location of GFP-positive cells and the colocalization with cellular markers were confirmed by 3D reconstructions of z series. For super-resolution imaging, a Zeiss LSM 880 Airy scan microscope (x63 objective lens) was used.

3D morphological analysis and cell counting

GFP^+-labeled cells were 3D reconstructed using the Imaris 8.4.1 software (Bitplane) or Neurolucida (MBF Bioscience). The Filament function in Imaris was used for neurite tracing and the Cell function was used for analyzing cell area and volume. Sholl plots were compiled from the 3-D vector-based Imaris datasets by using 10-μm increment concentric circles around the center of the soma. To count cells in images, the Cell counter function in Fiji was used, and the coordination of counted cells was exported to Excel files for further analyses. All numerical analyses were performed using Excel (Microsoft) and GraphPad Prism.

QUANTIFICATION AND STATISTICAL ANALYSIS

Statistical analyses were performed using R software, GraphPad Prism and Excel (Microsoft). p-values were determined by an unpaired Student's t-test, a Welch's t test, a Mann-Whitney U test, Kruskal-Wallis test or ANOVA. Boxplots with whiskers indicate minimum to maximum values, with box limits for 25^{th} to 75^{th} percentile, and a centerline for median.